Interaction of LL-37 with Model Membrane Systems of Different Complexity: Influence of the Lipid Matrix

E. Sevcsik,* G. Pabst,* W. Richter,† S. Danner,* H. Amenitsch,* and K. Lohner*
*Institute of Biophysics and Nanosystems Research, Austrian Academy of Sciences, Graz, Austria; and †Friedrich-Schiller-Universität Jena, Elektronenmikroskopisches Zentrum der Medizinischen Fakultät, Jena, Germany

ABSTRACT As the main difference between bacterial and mammalian cell membranes is their net charge, the focal point of consideration in many model membrane experiments with antimicrobial peptides is lipid headgroup charge. We studied the interaction of the human multifunctional peptide LL-37 with single phospholipid monolayers, bilayers, and bilayers composed of binary mixtures of the four phospholipid species predominantly used in model membrane experiments (phosphatidylcholine, phosphatidylethanolamine, phosphatidylglycerol, and phosphatidylserine). We found that 1), the effects on single lipid monolayers are not comparable to those on the corresponding bilayers; 2), there are four different effects of LL-37 on bilayers of the four lipids; 3), the preference of LL-37 for the specific lipids is roughly inversely related to chain packing density; and 4), in the binary lipid mixtures, one lipid—and not necessarily the charged one—generally governs the mode of lipid/peptide interaction. Thus, our results show that lipid net charge is not the decisive factor determining the membrane-perturbing mechanism of LL-37, but only one of several parameters, among them packing density, the ability to form intermolecular H-bonds, and lipid molecular shape, which emphasizes how profoundly the choice of the model system can influence the outcome of a study of lipid/peptide interaction.

INTRODUCTION

The rapid emergence of antibiotic-resistant bacterial strains necessitates the finding of therapeutic agents with a different mode of action but the same characteristics as conventional antibiotics, namely low toxicity and a broad spectrum of activity. Given these requirements, antimicrobial peptides (AMPs) represent good templates for a new generation of antibiotics. AMPs are a class of small, generally cationic and amphipathic peptides that kill bacteria with high potency and speed, suggesting that their mechanisms of action involve disruption of the cell membrane of the invading pathogen (1). Therefore, the effect of such peptides on membranes and the relevance of membrane lipid composition have been topics of interest for more than a decade. Artificial membranes that mimic mammalian and bacterial cell membranes, whether in the form of lipid monolayers, oriented bilayers, or vesicles, have become well-established model systems for the study of AMPs (2). Although it is clear that the biological activity of an AMP cannot directly be inferred from model membrane experiments, such studies provide a means to evaluate whether and how peptides interact with lipid membranes, which may be useful, for example, in developing new AMPs with enhanced properties. Well-known effects of AMPs on lipid bilayers include pore formation, micellization, binding to specific lipids, phase separation, induction or inhibition of nonlamellar phases, membrane thinning, and transversing the bilayer without disruption (for a review, see Lohner and Blondelle (3)).

The key to the effectiveness of AMPs as antimicrobial agents lies in the rather different composition of bacterial and mammalian cytoplasmic membranes. Erythrocyte membranes mainly contain phosphatidylcholine (PC), sphingomyelin, and cholesterol in the outer cytoplasmic leaflet, and are therefore charge-neutral at physiological pH (4). Cell surfaces of both Gram-positive and Gram-negative bacteria, on the other hand, comprise large amounts of negatively charged lipids, mostly lipoteichoic acids and lipopolysaccharides, respectively. Cytoplasmic membranes of Gram-negative bacteria are predominantly composed of phosphatidylethanolamine (PE) and, to a lesser extent, negatively charged phosphatidylglycerol (PG) and cardiolipin (5). In Gram-positive bacteria, the latter lipids are the main membrane constituents (6). The paradigm of AMP research is that the cationic peptides interact preferentially with the negatively charged bacterial membranes (and not at all, or less, with the charge-neutral host cell membranes). Therefore, in many studies of AMP/membrane interaction, the focal point of consideration is still lipid headgroup charge. Although this is undoubtedly an important parameter, restricting a study to charge effects means neglecting other membrane properties. Natural membranes contain a tremendous variety of different lipids with very diverse physicochemical properties that bestow certain attributes upon a membrane, such as, e.g., curvature strain, surface charge, and fluidity (7,8). A perfect model system would be sufficiently simple to allow conclusions to be drawn about the interaction of lipids and peptides

Submitted October 9, 2007, and accepted for publication January 23, 2008.

Address reprint requests to Eva Sevcsik, Institute of Biophysics and Nanosystems Research, Austrian Academy of Sciences, Schmiedlstrasse 6, 8042 Graz, Austria. Tel.: 43-316-4120-322; Fax: 43-316-4120-390, E-mail: Eva.Sevcsik@oeaw.ac.at.

Editor: Petra Schwille.

0006-3495/08/06/4688/12 $2.00

doi: 10.1529/biophysj.107.123620

on a molecular level while still retaining the basic characteristics of the membrane being modeled.

In this study we focus on the zwitterionic lipids PC and PE and the negatively charged lipids PG and PS, which are the phospholipid species predominantly used in model membrane experiments. Although both PC and PE are zwitterionic lipids, they differ in their molecular shape. PC, like PG, has a cylindrical shape, whereas fully hydrated PE contains less water and therefore has a less voluminous headgroup, leading to an inverted (truncated) cone shape of the molecule (9). A PS molecule carries a net charge of −1, like PG, but differs from PG in that this is the result of one positive and two negative charges. It also has a cylindrical molecular shape, but shares with PE the ability to engage in hydrogen-bonding (10). Structures of the phospholipids used in this study are shown in Fig. 1. Some membrane-active compounds have already been shown to interact differently with lipid systems carrying the same net charge. Although magainin 2 has the same binding affinity to PS as to PG, it is more effective at inducing leakage in PG than in PS liposomes (11). Arnt et al. (12) found that PE/PG vesicles were more sensitive than PS/PC vesicles to organic compounds mimicking host defense peptides, which is probably related to the propensity of these compounds to induce nonlamellar phases. The fish toxin pardaxin has a different effect on lipid bilayers of 1-palmitoyl-2-oleoyl-phosphatidylcholine (barrel-stave pore), dimyristoylphosphatidylcholine (surface-oriented peptide), and 1-palmitoyl-2-oleoyl-*sn*-glycero-3-phosphoethanolamine (cubic phase formation or micellization) (13). We have shown previously that the membrane-active peptides LL-37, PGLa, and melittin interact differently with PG and PC model membranes but that the mode of interaction is equally dependent on the lipid hydrocarbon chain length (14). Specifically, we found the formation of disk-like micelles for dimyristoylphosphatidylcholine and dipalmitoylphosphatidylcholine (DPPC), but a quasi-interdigitated phase for PGs and long-chain PCs in the presence of 4 mol % LL-37.

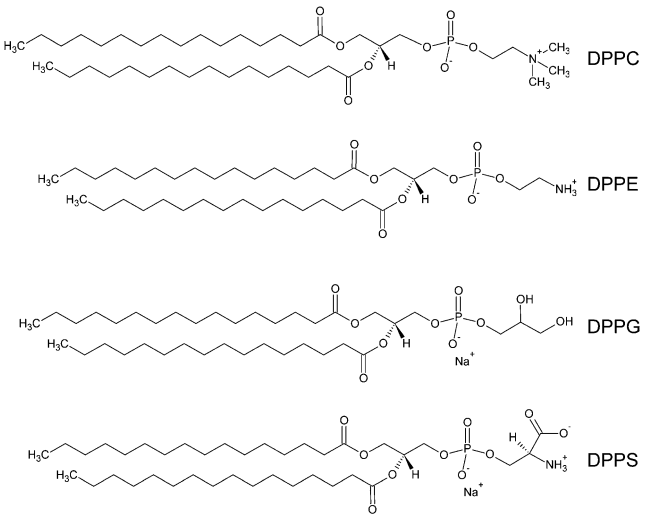

FIGURE 1 Structures of the four phospholipids used in this study.

In this study, we investigate the influence of the lipid headgroup on the interaction of LL-37 with model membranes of different complexity. The human cathelicidin LL-37 is a well-studied peptide that, in addition to its membrane activity, has been shown to participate in the inflammatory process by several means (for a review, see Durr et al. (15)). It comprises 37 amino acid residues, carries a net charge of +6 and adopts an amphipathic α-helix from residues 11–32 in aqueous solution at physiological conditions, as well as in the presence of lipids. A feature that distinguishes LL-37 from many other antimicrobial peptides, which act selectively on bacterial cells, is its cytotoxicity (16). On the basis of ATR-FTIR and ^{31}P NMR spectroscopy data of oriented bilayers, which indicate that LL-37 (up to 5 mol %) lies roughly parallel to the bilayer plane in PC, PC/cholesterol, and PC/PG multilayers and does not penetrate deeply into the hydrophobic core of the membrane, a nonpore carpet mechanism has been suggested (17,18). In this study, we use monolayer insertion, differential scanning calorimetry, small- and wide-angle scattering, electron spin resonance spectroscopy, and electron microscopy to evaluate peptide binding to monolayers and the effect on the structure and thermotropic phase behavior of single-component phospholipid bilayers and bilayers composed of binary lipid mixtures. We find that 1), effects on the single lipid monolayers are not comparable to the effects on the corresponding bilayers; 2), four different modes of interaction exist for LL-37 with bilayers of the four phospholipids used (DPPC, dipalmitoylphosphatidylglycerol (DPPG), dipalmitoylphosphatidylserine (DPPS), and dipalmitoylphosphatidylethanolamine (DPPE)); and 3), there are significant differences in the mode of lipid/peptide interaction between the binary lipid mixtures PC/PG, PE/PG, and PC/PS, which all carry the same net charge.

MATERIALS AND METHODS

Materials

LL-37 was purchased from Peptide Specialty Laboratories (Heidelberg, Germany). Peptide purity was >95%. Phospholipids were purchased from Avanti Polar Lipids (Alabaster, AL) and used without further purification. Stock solutions of all lipids were prepared in chloroform/methanol (9:1 v/v) and stored at −18°C. Purity (>99%) was checked before and after experiments by thin-layer chromatography showing a single spot using $CHCl_3$/CH_3OH/NH_3 (25% in water) (65:35:5 v/v/v) as mobile phase and detection with the phosphorus-sensitive reagent molybdenic acid.

Preparation of liposomes

Appropriate amounts of phospholipid and peptide stock solutions were dried under a stream of nitrogen, stored in vacuum overnight, and dispersed in sodium phosphate-buffered saline (PBS) (20 mM PBS, 130 mM NaCl, pH 7.4). Hydration at a temperature above the phase transition of the respective

phospholipids was intermitted by vigorous vortex mixing. For electron spin resonance (ESR) experiments, a 16-doxyl stearic acid (16-DSA) spin label (Sigma, St. Louis, MO) dissolved in ethanol was added before solvent evaporation (lipid/DSA molar ratio 150:1).

Monolayer experiments

Measurements were performed using a thermostatted Langmuir film balance trough Type 601 (Nima Technology, Coventry, United Kingdom) equipped with two movable barriers and a Wilhelmy plate surface-tension measuring system. The trough was filled with PBS and, before each experiment, contaminating surface-active impurities were removed by simultaneous sweeping and suction of the interface. After this cleaning, 50 μL of a 1-mg/mL stock solution of the respective lipid in chloroform/methanol (9:1 v/v) was gently deposited at the air-water interface using a Hamilton microsyringe with the barriers fully open. After 10 min for solvent evaporation, lipid films were compressed at a constant rate of 25 cm^2/min to a final surface pressure of 15 mN/m and 30 mN/m, respectively. After equilibration, peptide was injected into the subphase and changes of area/molecule or surface pressure were recorded using software provided by Nima. Experiments were performed at 23°C.

Small- and wide-angle x-ray scattering

X-ray scattering experiments were performed with a small- and wide-angle x-ray (SWAX) camera equipped with two linear, position-sensitive detectors (HECUS X-ray Systems, Graz, Austria) allowing simultaneous sampling of diffraction data in the small- and wide-angle regions. The camera was mounted on a sealed-tube x-ray generator (Seifert, Ahrensburg, Germany), which was operated at 2 kW. CuKα radiation ($\lambda = 1.542$ Å) was selected using a Ni filter in combination with a pulse height discriminator. After equilibrating the samples for 10 min at the respective temperature, diffractograms for the small- and wide-angle regions were recorded with exposure times of 3600 s each. Lipid dispersions (50 mg/mL) were measured in a thin-walled, 1-mm-diameter quartz capillary in a steel cuvette (Anton Paar, Graz, Austria), which was inserted into a brass block. Automatic temperature control was provided by a programmable Peltier unit. Angular calibration of the scattered intensities in the small-angle regime was performed with silver stearate and in the wide-angle regime with *p*-bromo-benzoic acid. Background corrected SAXS data were evaluated in terms of a global analysis technique (19). In the applied model, the bilayer electron-density profile is given by the summation of three Gaussian distributions, two describing the electron-dense headgroup region at $\pm z_H$ and one at the center of the bilayer ($z = 0$) accounting for the trough at the methyl terminus of the hydrocarbon chains. From the fitting parameters, we define the phosphate-phosphate distance, $d_{PP} = 2z_H$, as a measure for the membrane thickness.

PE/PG diffraction patterns were recorded at the Austrian SAXS beamline Elettra (Trieste, Italy) (20) using a photon energy of 8 keV and two one-dimensional position-sensitive detectors to cover scattering vectors $q = 4\pi\sin(\theta/\lambda)$ from 0.01 $Å^{-1}$ to 0.5 $Å^{-1}$ and 0.7 Å to 1.9 Å, respectively. Angular calibration of the scattered intensities in the small-angle regime was performed with silver behenate and in the wide-angle regime with *p*-bromo-benzoic acid. Temperature was controlled by a programmable circulating water bath (Unistat CC, Huber, Offenburg, Germany). Temperature was increased at a rate of 0.25°C/min and scattering patterns were recorded for 60 s.

From WAXS data we calculate the area/hydrocarbon chain in the case of orthorhombic packing from (21)

$$A_C = \frac{4\pi^2}{\sqrt{q_{20}^2 q_{11}^2 - q_{20}^4/4}}, \quad (1)$$

and for hexagonally packed hydrocarbon chains we apply (9)

$$A_C = \frac{8\pi^2}{\sqrt{3}\, q_{11}^2}. \quad (2)$$

q_{hk} corresponds to the position of the hydrocarbon chain reflections in the WAXS regime with the Miller indices h and k. The lateral area/lipid for untilted chains is $A = 2A_C$ and

$$A = \frac{2A_C}{\cos\theta_t} \quad (3)$$

in the case of an orthorhombic lattice, where θ_t is the average chain tilt (see Table 4).

Electron spin resonance spectroscopy

ESR spectra were recorded on an X-band ECS106 spectrometer (Bruker, Rheinstetten, Germany) cooled with liquid nitrogen. Measurement conditions were: 3390 G center field, 100 G sweep width, 1 G modulation amplitude, 50 kHz modulation frequency, and 10 mW microwave power. An accumulation of 10 scans yielding acceptable signal/noise ratio was used throughout the experiments. Measurements were carried out at 9°C. Spectral parameters were determined using Win-EPR Software. The maximum hyperfine splitting, A_{II}, of the ESR spectra was used as a measure of the motional restriction of the spin label. Sample concentration was 30 mg/mL.

Differential scanning calorimetry

Differential scanning calorimetry (DSC) studies were performed with a Microcal VP-DSC high-sensitivity differential scanning calorimeter (Microcal, Northampton, MA). Scans were recorded at a constant rate of 30°C/h. Sample concentration was 1 mg/mL. Using Microcal Origin software, calorimetric enthalpies were calculated by integrating the peak areas after baseline adjustment and normalization to the mass of phospholipid. The phase transition temperature was defined as the temperature at the peak maximum.

Freeze-fracture transmission electron microscopy

Dispersions of the samples (5 mg/ml) with and without addition of 20% (v/v) glycerol were equilibrated and quick-frozen from the temperatures as indicated. A small amount of the samples was sandwiched between two copper profiles (BAL-TEC, Balzers, Liechtenstein), as used for the double-replica technique, and frozen by plunging the sandwiches immediately into liquefied ethane-propane-mixture (1:1 v/v) cooled in liquid nitrogen. Fracturing and replication were performed at −150°C in a BAF 400T freeze-fracture device (BAL-TEC) equipped with electron guns and a film-sheet thickness monitor. For replication, at first *Pt*(*C*) was evaporated under an angle of 35° followed by *C* under 90°. The replicas were placed on copper grids (Mesh 400), cleaned with a chloroform-methanol mixture, and examined in an EM 900 electron microscope (Zeiss, Oberkochen, Germany).

RESULTS

Effect of LL-37 on single component monolayers

Although water-soluble, LL-37 accumulates at the air-water interface when injected into a buffer subphase due to its amphipathic structure. The peptide builds a stable monolayer that can be compressed up to a surface pressure (π) of 24 mN/m before collapse (data not shown), which is roughly compa-

rable to the collapse pressure reported by Neville et al. (22). Consequently, when LL-37 is injected into the bulk subphase underneath a lipid monolayer, any increase of π to >24 mN/m can be considered to involve lipid/peptide interaction. Pure DPPC, DPPG, DPPE, and DPPS build stable monolayers that begin to collapse at ~60 mN/m (data not shown).

In our experimental setup, lipid monolayers were compressed to a surface pressure of either 15 mN/m or 30 mN/m. After observing film stability over 10 min, 8.9 nmol peptide (corresponding to a lipid/peptide molar ratio of 25:1) was injected into the subphase. Two kinds of experiments were conducted. In the first type, the film area was kept constant and the increase of surface pressure was recorded. In the second setup, the surface pressure was held constant and changes of area/molecule were monitored. Maximum surface pressures (π_{max}) reached upon peptide insertion, as well as changes of area at a constant π of 30 mN/m, are presented in Table 1. For DPPC and DPPE monolayers, constant area isotherms with an initial pressure of 15 mN/m show an increase of surface pressure to 24 mN/m upon peptide injection, which corresponds to the collapse pressure of the peptide itself. At 30 mN/m (which is considered to be physiologically relevant (23)), the peptide does not insert into either DPPC or DPPE monolayers, which is in agreement with previous data (22). In contrast, LL-37 integration to surface pressures >30 mN/m can be observed for DPPG and DPPS monolayers, and at a constant pressure of 30 mN/m, LL-37 injection causes an increase of area for the two monolayers of 35% and 29%, respectively. These experiments clearly show that the incorporation of LL-37 into DPPG and DPPS monolayers is not limited to the collapse pressure of the peptide itself, as is the case with DPPC and DPPE, which is presumably due to electrostatic interaction of the positively charged peptide with the negatively charged lipid headgroups.

Effect of LL-37 on single-component bilayers

The effects of LL-37 on the thermotropic phase behavior and structural parameters of all the lipid systems investigated are summarized in Tables 2 and 3. The thermotropic phase behavior of the zwitterionic DPPE is characterized by a single, cooperative transition at 63.4°C, which is not affected by the presence of 4 mol % LL-37. Consistently, phosphate-phosphate distance (d_{PP}), lamellar spacing (d) (Table 2), and WAXS pattern of DPPE are unaltered in the presence of LL-37 in the gel as well as the fluid phase.

Although no interaction was observed with DPPC monolayers, we reported previously (14) that addition of 4 mol % LL-37 to DPPC vesicles leads to a disintegration of the multilamellar lipid arrangement and gives rise to the formation of disk-like micelles with diameters around 30 nm. We proposed a bicycle-tire model, where the hydrophobic rims of a lipid disk are covered by peptide molecules (see Fig. 5 *C*). A rough calculation of the lipids/peptide at this disk size, assuming nonoverlapping peptide helices with a length of 5.5 nm (corresponding to an α-helix of 37 amino acids) and an area/lipid of 0.5 nm^2, gives 33:1, suggesting that at 4 mol %, most, or even all, of the peptide is situated at the disk rims.

The heat capacity function of DPPS liposomes is characterized by a highly cooperative main transition at 52.6°C (Table 2 and Fig. S1 *A* in the Supplementary Material) and a minor transition at 53.5°C, which decreases upon rescans and probably represents a moiety of lipid that is less hydrated (24,25). Upon addition of 4 mol % LL-37, neither the total transition enthalpy nor the temperature is affected significantly. The enthalpy of the transition at 53.5°C is initially nearly comparable to the enthalpy of the main transition but decreases to 15% of the total enthalpy upon rescans. This second transition may be due to shielding of negative charges and/or displacement of water by peptide binding, leading to a dehydration of the headgroups (26). The SAXS pattern of DPPS shows a quasi-Bragg peak characteristic of positionally weakly correlated bilayers of oligolamellar vesicles (Table 3 and Fig. S1 *C*). The corresponding WAXS data show a single symmetric peak centered at $q = 1.5$ $Å^{-1}$, characteristic of hexagonally packed all-*trans* lipid acyl chains oriented perpendicular to the bilayer plane (27). The presence of 4 mol % LL-37 induces a slight increase of the lamellar spacing from 109 Å to 117 Å, which is accompanied by an increase of positional correlations. We do not find a significant effect of the peptide on d_{PP} (Table 3), WAXS

TABLE 1 Maximum surface pressure, π_{max}, and increase of area per molecule, $\Delta A/A$, observed 200 min after injection of LL-37

	π_{max} (mN/m)*	$\Delta A/A$ (%)†
DPPC	24	0
DPPG	34	35
DPPE	24	0
DPPS	33	29
DPPC/DPPG	31	17
DPPC/DPPS	27	4
DPPG/DPPE	29	11

Subphase was PBS, pH 7.4, at $T = 23$°C.
*Initial surface pressure $\pi_0 = 15$ mN/m.
†Constant surface pressure $\pi = 30$ mN/m.

TABLE 2 Main transition temperatures, T_m, and total transition enthalpies, ΔH_m, in the absence and presence of 4 mol % LL-37

	T_m (°C)		ΔH_m (kcal/mol/°C)	
	Pure	+LL-37	Pure	+LL-37
DPPC	41.5	42.8	8.2	4.0
DPPG	40.7	42.6	9.3	10.2
DPPE	63.4	63.4	8.1	8.5
DPPS	52.6*	52.7*	10.0	9.8
DPPC/DPPG	41.4	42.6	8.5	7.9
DPPC/DPPS	45.6	45.3	9.1	6.7
DPPG/DPPE	54.6	56.2*	10.1	10.6
DPPG/DPPS	47.6	47.5*	9.4	9.1

*Peak splitting.

TABLE 3 Lamellar spacing, *d*, and phosphate-phosphate distance d_{PP} in the gel and fluid phases in the absence and presence of 4 mol % LL-37

	Gel (T_m − 15)°C				Fluid (T_m + 10)°C			
	Pure		+ LL-37		Pure		+ LL-37	
Lipid	*d*	d_{PP}	*d*	d_{PP}	*d*	d_{PP}	*d*	d_{PP}
DPPC	66	43.4	–	44.0	66	38.2	74	37.4
DPPE	65	49.5	64	50.1	53	40.7	53	41.5
DPPG	110	44.6	–	31.1	–	38.1	–	35.7
DPPS	109	49.7	117	48.9	95	41.6	–	n.d.[†]
DPPG/DPPE	117	48.3	84*/122	n.d.[†]	113	39.0	–	39.2
DPPC/DPPG	103	44.0	–	33.7	90	39.0	–	35.9
DPPC/DPPS	–	46.4	82*/–	47.2	–	40.9	–	38.0
DPPG/DPPS	122	47.6	–	48.2	–	38.6	–	36.1

*T_m − 45°C.
[†]Not determined because application of the fitting model did not yield unequivocal results.

pattern, or ESR spectra (Fig. S1). In accordance with DSC data these results suggest that the peptide does not penetrate into the hydrophobic core of the bilayer but rather binds to the surface, where it shields the negative charges, leading to an increase of positional correlations between the bilayers, which are, however, lost in the fluid phase due to increased thermal undulations (28).

We reported previously (14) that the effect of LL-37 on DPPG, the fourth lipid used in this study, is characterized by a drastically reduced bilayer thickness, an increased order parameter at the terminal methyl group of the hydrocarbon chains, and a stabilization of the gel phase. From these data we concluded the formation of a quasi-interdigitated gel phase in the presence of peptide. Above the T_m, we found that LL-37 induced a thinning of the bilayer by 2.4 Å, which is more pronounced than that observed for DPPC (0.8 Å) (Table 3).

Effect of LL-37 on monolayers of lipid mixtures

Binary lipid mixtures are often used to mimic complex biological membranes, e.g., PE/PG, PC/PG, and, less often, PC/PS, for cytoplasmic bacterial membranes. Thus, to evaluate whether LL-37 shows a preferential interaction with one of the lipids when present in a more complex mixture, we performed experiments with such binary equimolar lipid mixtures. We found that π_{max} reached upon insertion of LL-37 is highest for PC/PG, slightly lower for PE/PG, and even lower for PC/PS (Table 1). These results correspond well to the increases of area observed at a constant surface pressure of 30 mN/m, which are between the values observed for pure charged and uncharged lipids and decrease in the order PC/PG > PE/PG > PC/PS.

Effect of LL-37 on bilayers of lipid mixtures

DPPE/DPPG

Addition of 4 mol % LL-37 results in a significant alteration of the heat-capacity function of the equimolar PE/PG mixture, which involves a phase separation, most likely into peptide-rich and peptide-poor domains (Fig. 2 *A* and Table 2). Presumably, the cationic peptide interacts preferentially with the negatively charged DPPG, thereby depleting it from the lipid mixture and forming peptide-enriched PG domains that melt at lower temperatures. This leads to an elevated temperature of the main phase transition owing to the increased content of PE molecules in those domains. This assumption is supported by the fact that experiments with the pure phospholipids showed a strong interaction of LL-37 with DPPG but none with DPPE. In addition, a low-temperature transition at 29°C appears. Moreover, a small contribution to the heat capacity is still observed between the low temperature and the main transition. This uncooperative transition suggests that there is an ongoing structural rearrangement of the lipid mixture within this temperature range.

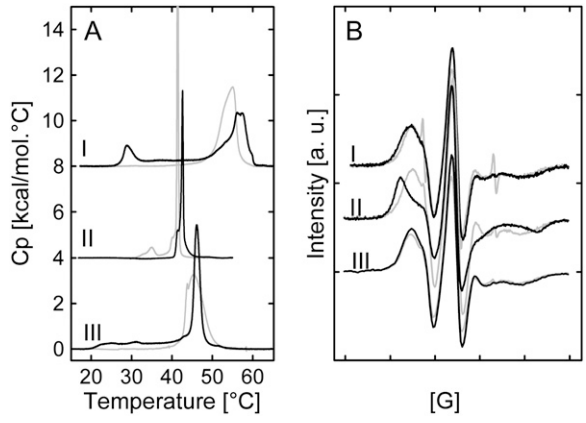

FIGURE 2 (*A*) Thermograms of PE/PG (I), PC/PG (II), and PC/PS (III) in the presence of 4 mol % LL-37 (*solid lines*) recorded at a scan rate of 30°C/h. The corresponding thermograms of the pure lipid mixtures are shown in gray. Third heating scans are shown. (*B*) ESR spectra of a 16-DSA spin label in vesicles of PE/PG (I), PC/PG (II), and PC/PS (III) in the presence of 4 mol % LL-37 (*solid lines*). The corresponding spectra of the pure lipid mixtures are shown in gray. $T = 9$°C; total scan width, 100 G.

ESR spectra in the presence of peptide do not differ significantly from those of the pure lipid mixture (Fig. 2 *B*). Pure PE/PG exhibits a scattering pattern characteristic of positionally weakly correlated bilayers, and correlation increases upon the addition of peptide (Fig. S2). Due to insufficient data quality above $q = 0.2$ Å^{-1}, application of the fitting model did not yield unequivocal values for d_{PP}. As shown in Fig. 3, the phase transition at 29°C is associated with the disappearance of a phase with a lamellar distance of 84 Å and the formation of a new phase with $d = 122$ Å. At the same time the WAXS peak position changes progressively and without any discontinuities between 22°C and 40°C from $q = 1.52$ Å^{-1} to $q = 1.5$ Å^{-1} (data not shown), indicating no major structural rearrangement of the hydrocarbon chain packing at 29°C. The transition at 29°C observed in the thermogram may result from a melting of a part of the lipids (most likely, peptide-associated PG), which leads to undulations of the bilayers, repulsion, and, in consequence, an increase of the lamellar repeat. Upon passing through the T_m, interbilayer positional correlations are lost abruptly and the system exhibits pure diffuse small-angle scattering (Table 3 and Fig. S2). This indicates an unbinding transition due to thermal undulations as previously observed for POPE/POPG mixtures (28).

We performed freeze-fracture transmission electron microscopy (FFTEM) to get additional clues on the mode of action of LL-37 from its influence on the morphology of the PE/PG mixture. Whereas the pure mixture forms multilamellar vesicles of different sizes (as observed by light microscopy, data not shown), the vesicular structure is destroyed in the presence of LL-37 and plane bilayer fragments of different size (50–200 nm) and shape are formed (Fig. 4). At 10°C, in good agreement with SAXS data, the fragments tend to aggregate and stack into lamellar arrangements with repeat distances of ~9 nm corresponding to those from SAXS data. At 40°C, the bilayer fragments appear more circular in shape and the repeat distance, as well as the number of solitary disks, increases. In the fluid phase, in accordance with SAXS data, only solitary disks with diameters between 15 and 100 nm can be observed, some of which have partially fused into larger bilayer sheets.

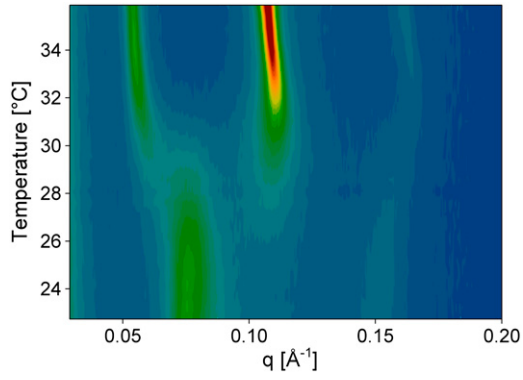

FIGURE 3 Contour plot of SAXS patterns of PE/PG with 4 mol % LL-37 as a function of temperature. Highest intensities are colored in dark red, lowest in blue.

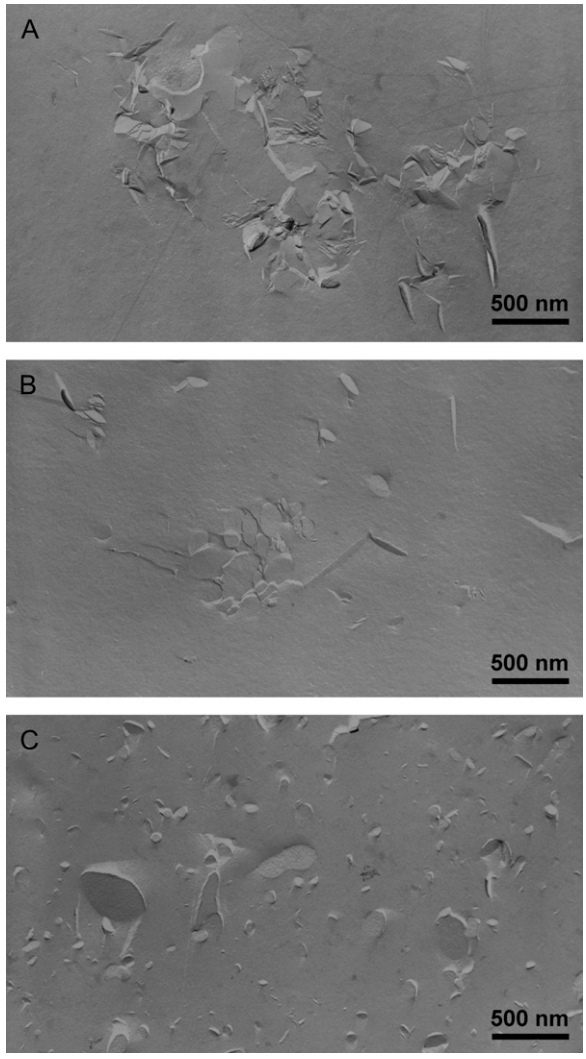

FIGURE 4 FFTEM images of PE/PG in the presence of 4 mol % LL-37. Freezing from (*A*) 10°C, (*B*) 40°C, and (*C*) 65°C. Scale bar, 500 nm.

DPPC/DPPG

When DPPC, instead of DPPE, is mixed with DPPG, the overall charge of the lipid system does not change, as both PE and PC are zwitterionic lipids, however, we find a totally different mode of lipid/peptide interaction. Fig. 2 *A* shows the thermograms of liposomes of an equimolar DPPC/DPPG mixture in the absence and presence of 4 mol % LL-37. The thermogram of the pure lipid mixture is characterized by a symmetric peak at 41.4°C, corresponding to the highly cooperative main phase transition ($P_{\beta'} \rightarrow L_{\alpha}$) and a pretransition related to the formation of a ripple phase ($L_{\beta'} \rightarrow P_{\beta'}$) at 35.0°C. Upon addition of LL-37, the pretransition is abolished and the main phase transition is shifted to 42.6°C, indicating a stabilization of the gel phase as already observed

for quasi-interdigitated DPPG bilayers in the presence of LL-37 (14). The shoulder at 41.4°C suggests that there is still some noninterdigitated lipid left, probably DPPC. ESR spectra show a pronounced decrease of 16-DSA mobility, indicating that the spin label, which probes the region near the terminal methyl groups, is more motionally restricted and behaves like a label close to the interface, encouraging the assumption of a quasi-interdigitated bilayer (Fig. 2 *B*). Further support for this interpretation is provided by SAXS data showing that the presence of 4 mol % LL-37 provokes a decrease of d_{PP} from 41.2 Å to 33.7 Å (Table 3). These data indicate that DPPC, although not prone to form a peptide-induced quasi-interdigitated phase by itself, can be largely incorporated into an interdigitated DPPG bilayer even in an equimolar mixture. As already observed for DPPG with LL-37, we find a thinning of the bilayer by 3.1 Å at 4 mol % LL-37 in the fluid phase.

DPPC/DPPS

The thermogram of a DPPC/DPPS equimolar mixture is characterized by a broad transition centered at 45.6°C, suggesting nonideal mixing of these components (Fig. 2 *A* and Table 3). Addition of 4 mol % LL-37 provokes an increase of transition cooperativity and symmetry, a minor increase of T_m, and a pronounced decrease of transition enthalpy. At ~20°C, the onset of a very weakly cooperative transition can be observed. ESR spectra of the mixture in the absence and presence of peptide are virtually superimposable (Fig. 2 *B*). Electron microscopy images show disk-like micelles with diameters ranging from 20 to 40 nm at 15°C (Fig. 5 *B*), very similar to what was observed for pure DPPC (14). Fig. 5 *C* shows a sketch of a lipid disk surrounded by peptide molecules, as we proposed previously for DPPC (14) and now also assume for PC/PS. Above the onset of the transition, the disks start to merge and form lamellar sheets, indicating that chain melting is involved in the fusion of the micelles. As can be inferred from SAXS data, this process is associated with a loss of the weak interbilayer positional correlations observed at 15°C, whereas WAXS data indicate that the lipid packing remains largely unaltered (Fig. 5 *A*). The incongruities between the SAXS pattern and the fits observed at 35°C may be explained by the existence of two populations (disks and extended bilayers) with different structural parameters or by the formation of asymmetric bilayers (29). On the whole, the effect of LL-37 on PC/PS is very much like that on pure PC, indicating that the mode of interaction is clearly dominated by PC rather than PS.

DISCUSSION

As the main difference between bacterial and mammalian cell membranes is their net charge, the focus of many model membrane experiments with AMPs has been on electrostatics. However, surface charge does not necessarily play the dominant role in the interaction of cationic peptides with model membranes. We reported previously that the membrane-active peptides LL-37, PGLa, and melittin induce the

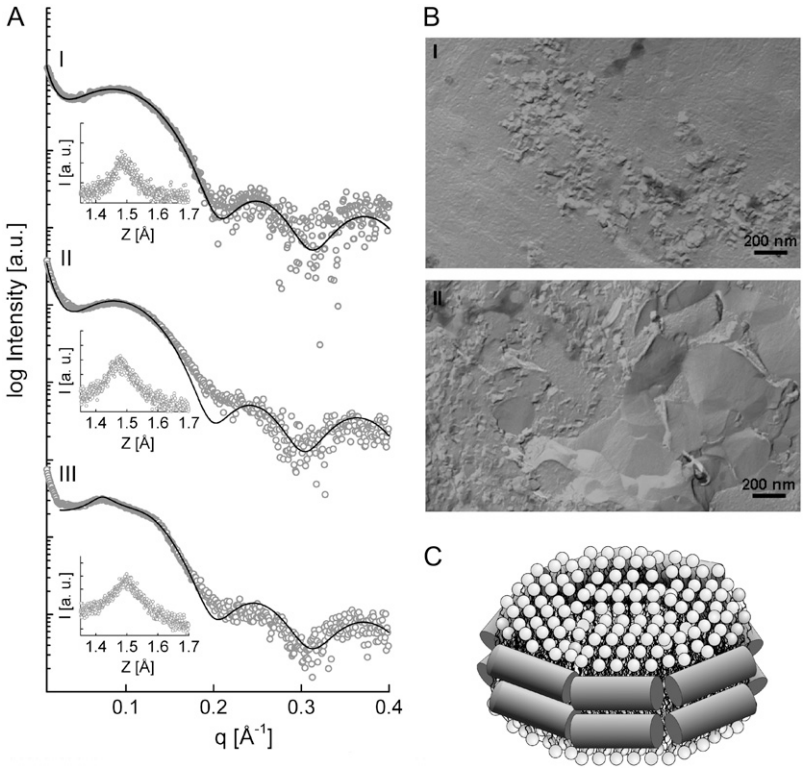

FIGURE 5 (*A*) SAXS pattern of PC/PS in the presence of 4 mol % LL-37 at 10°C (I) and 35°C (II) and in the absence of LL-37 at 35°C (III). Solid lines show full-*q*-range fits. WAXS patterns are shown in the insets. (*B*) FFTEM images of PC/PS in the presence of 4 mol % LL-37. Freezing from 10°C (I) and 35°C (II). Scale bar, 200 nm. (*C*) Schematic drawing of a lipid disk surrounded by LL-37 as proposed for DPPC in (14) and here for PC/PS.

formation of a quasi-interdigitated phase in DPPG model membranes, whereas for DPPC, either micellization or no effect was observed (14). Intriguingly, for the same peptides, we found quasi-interdigitated phases with long-chain PCs, indicating that by increasing chain length, the effect of headgroup charge can be overruled. In this study, we investigated the effect of LL-37 on DPPC, DPPG, DPPS, DPPE, and mixtures thereof to evaluate the influence of the lipid headgroup on lipid/peptide interactions in model systems of different complexity.

Four lipids, four effects

A schematic overview of the macroscopic phases observed for the lipid/peptide systems investigated is presented in Fig. 6. The main findings are:

1. Effects of LL-37 on lipid monolayers cannot be translated into effects on bilayers, and vice versa. The interaction of LL-37 with single-component lipid monolayers seems to be governed by electrostatic effects. When the mode of interaction involves a three-dimensional rearrangement of the peptide/lipid system (such as formation of peptide-sheathed lipid disks), the monolayer system, in contrast to the bilayer, is not affected, due to a lack of a driving force for interaction.
2. Although the effects on all the bilayer systems are diverse, they can be divided roughly into four categories: 1), interdigitation; 2), formation of bilayer disks; 3), surface binding; and 4), no interaction.
3. The preference of LL-37 for the specific lipids, as concluded from the extent of interaction with single-lipid systems, as well as from the role of the lipids in the binary mixtures, decreases in the following order: PG $\geq$ PC $>$ PS $>$ PE (note that this correlates roughly with an increase of chain-packing density).
4. In the binary lipid mixtures, one lipid generally governs the mode of lipid/peptide interaction (with the exception of the PE/PG mixture), and this is not necessarily the charged lipid.

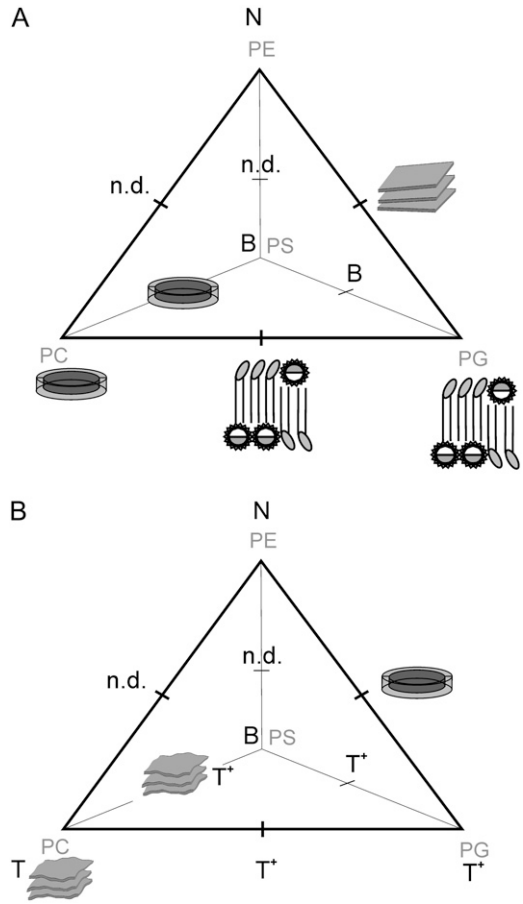

FIGURE 6 Schematic diagram showing the effect of LL-37 on the phospholipids DPPC, DPPE, DPPG, and DPPS and binary mixtures thereof in the gel phase (*A*) and in the fluid phase (*B*). N, no effect; B, surface binding; T, thinning; T^+, major thinning (>2Å). Disk-like micelles, quasi-interdigitated phases, bilayer fragments, and disks fused to extended bilayers are shown as sketches.

An overview of some basic characteristics of the lipids and their interaction with LL-37 is presented in Table 4. DPPC and DPPG bilayers differ in net charge; however, they share some basic bilayer properties (e.g., chain tilt of ~30° at physiological pH, similar thermodynamic behavior, not very tight chain packing, cylindrical molecular shape of lipids, etc.) (30–32). Although both are zwitterionic, PC and PE bilayers are characterized by significantly different structural and dynamical parameters (33,34). PE bilayers are more rigid, more tightly packed, and more highly ordered than PC, and the hydrocarbon chains of PE molecules are untilted because of a smaller headgroup and lower hydration (9,35–37). The lower hydration arises from the ability to form hydrogen bonds with phosphate and carbonyl O atoms from adjacent PEs. Owing to their inverted cone shape, PEs may form nonlamellar phases (34). Huang and co-workers found that PE inhibits membrane thinning and pore formation in PC bilayers by melittin and alamethicin, and they proposed that the peptides fill the volume in the headgroup region, which was voided by the replacement of PC by PE (38,39). A similar scenario can be envisioned for LL-37, but it seems rather unlikely that the introduction of a highly charged molecule in the headgroup region of PE would not affect the lamellar spacing. Probably, the too tightly packed PE bilayer and the H-bonds that would have to be overcome make an insertion into the hydrophobic core of the bilayer unfavorable.

Lewis and McElhaney have already speculated that PS may be able to bestow characteristics upon a lipid bilayer that are unrelated to its negative charge per se (40). In contrast to the singly negatively charged PG, the PS headgroup contains three charged moieties at neutral pH, two negative and one

TABLE 4 Basic lipid properties and effects of LL-37 at physiological conditions

	PC	PG	PS	PE
Net charge	0	−1	−1	0
Molecular shape/curvature (from Israelachvili et al. (50))	Cylindrical/0	Cylindrical/0	Cylindrical/0	Truncated cone/negative
Chain tilt θ_t*	31.6°, from (51)	29.5°, from (31)	–	–
H-bonding ability	No	No	Yes	Yes
Headgroup area A*†	48.1 Å^2	47.1 Å^2	40.6 Å^2	40.3 Å^2
Effect of LL-37*	Disk-like micelles with peptide rim	Quasi-interdigitation	Surface binding, unperturbed bilayer	None
Effect of LL-37‡	Fused disks, minor thinning	Major membrane thinning	Unbinding of bilayers	None

*Gel phase (25°C).
†Calculated from WAXS data.
‡Fluid phase.

positive, that are available for interaction with neighboring lipids as well as peptides (Fig. 1). Similar to PE, PS headgroups can engage in intermolecular hydrogen-bonding and act to compress the bilayer laterally, leading to tighter chain packing than exhibited by PG and PC, which is also reflected in the higher chain melting temperature (40,41). LL-37 can be incorporated into PG as well as PS monolayers up to a surface pressure of ~35 mN/m. However, LL-37 can only penetrate into PG bilayers, the driving force being the reorganization of the bilayer to the quasi-interdigitated structure. In PS bilayers, on the other hand, this reorganization does not take place. Moreover, as the serine carboxyl group of PS extends further toward the bulk water phase than the glycerol phosphate group, it is likely that LL-37 does not penetrate far into the interface because it is held back at the bilayer surface. The cationic peptide partially shields the negative charges (and possibly dehydrates the headgroups) leading to the increased interbilayer positional correlations observed in the SAXS experiments. Interaction with PG, but not at all, or less, with PS, was also shown for other membrane-active peptides. Volles et al. reported that dioleoyl-PS vesicles were not disrupted by α-synuclein, a peptide linked to Parkinson's disease, whereas dioleoyl-PG vesicles were disrupted—probably for the same reasons (42). PG-1 was shown to interact differently with the three acidic phospholipids DPPG, DPPS, and DPPA, which all carry the same net charge of −1 and the same hydrocarbon chains (24). This diverse interaction was ascribed to different structural features of the phospholipid headgroups and hydrocarbon chain packing.

Effects on the lipid mixtures

In contrast to the single-component systems, where electrostatics clearly dominate the peptide/monolayer interaction, significant differences between the monolayers of binary mixtures can be observed. The ability of LL-37 to insert decreases from PC/PG over PE/PG to PC/PS, which, as all of these mixtures carry the same net charge, most likely reflects the penetrability of the interface. The packing density of PC/PG is lower than for PE/PG and PC/PS. This is probably due to the H-bonding ability of PE and PS implicating a more tightly packed interface. In the case of PC/PS, LL-37 might be held back at the carboxyl group of PS, as already speculated for pure DPPS, which would additionally impede peptide insertion.

In general, the tendencies of lipid/peptide interaction observed in the single-lipid experiments are largely maintained in the lipid mixtures, with one lipid taking the dominant role. As we find a quasi-interdigitated phase in the PC/PG mixture, PG seems to govern the interaction of LL-37 with this system. It is interesting that when PC is replaced by PE, the lipid mixture reacts totally differently (i.e., forming stacks of bilayer fragments) to the presence of LL-37. At first glance, PE, with its small headgroup, might appear to be less prone to interdigitate, which is certainly true for a normal interdigitated phase. However, in the quasi-interdigitated phase described for LL-37, we also find a decreased headgroup area for PG (presumably due to a change of the orientation of the headgroup from horizontal to vertical), since the peptide, not a lipid headgroup, covers the tails of the hydrocarbon chains (14). Indeed, earlier findings from Boggs et al. (43) indicate that ~20 mol % DPPE, as well as DPPC, can be incorporated into the interdigitated bilayer of DPPG/polymyxin B (5:1). However, we are not aware of any substance or condition that induces interdigitation in pure PE bilayers (with the exception of mixed-chain PEs (44)). Considering these data, it is at present difficult to explain why an interdigitated phase is induced in the PC/PG but not in the PE/PG mixture. As mentioned above, PC and PG have rather similar characteristics, leading to nearly ideal mixing of these lipids (45). Owing to differences in chain tilt and molecular shape, one would expect a tendency for demixing for PE and PG, but experimental data, as well as molecular dynamics simulations, suggest hydrogen-bonding between PE and PG leading to the formation of mixed pairs (46,47). Since the PG phosphate group is engaged in hydrogen-bonding, it may be less available for peptide interaction, which might contribute to the different behavior of the PE/PG mixture in the presence of

LL-37. Furthermore, LL-37 induces a quasi-interdigitated phase in DSPC, indicating that the PC headgroup per se does not counter interdigitation (14).

Although there are similarities in the interaction of LL-37 with PE/PG on the one hand and PC and PC/PS on the other hand, there are still considerable differences. In PC and PC/PS, the disk size seems to be adjusted in such a way that most or all of LL-37 covers the hydrophobic disk rims. In contrast, assuming a mean diameter of 150 nm for the larger PE/PG bilayer fragments, the lipid/peptide ratio necessary for the hydrophobic disk rims to be covered by peptide would be >150:1. This indicates that at 4 mol %, the peptide is hardly located entirely at the rims of the bilayer fragments, but also resides in the bilayer, where it induces a phase separation by preferentially interacting with PG, leading to PE-enriched higher-melting domains, as observed in DSC experiments. At present, we do not have a satisfactory explanation for the thermodynamic and structural behavior of the PE/PG mixture in the presence of LL-37. Although undulations resulting from partial melting of the lipids in the course of the low-temperature transition might cause the stacked bilayers to move farther apart, and finally lead to their unbinding in the fluid phase, the role of the peptide in inducing the sample morphologies observed at the different temperatures remains to be elucidated.

When comparing the PC/PG and PC/PS mixtures, it is interesting that in the former case, the charged component plays the dominant role, whereas in the latter mixture, the mechanism of interaction is governed by the uncharged lipid. In this case, hydrophobic interactions might outweigh electrostatics, since the PC/PS mixture has a lower surface-charge density and packs less tightly than pure PS, which might facilitate peptide penetration into the hydrocarbon chain region. Intriguingly, in a PG/PS mixture, PS seems to dominate the mode of lipid/peptide interaction as it counteracts the formation of an interdigitated bilayer, as concluded from SWAXS, ESR, and DSC experiments (Table 2 and 3). This model system displays the highest surface-charge density of the binary lipid mixtures investigated. It can be speculated that the peptide binds preferentially to PS owing to the easier accessibility of the serine carboxyl group, and does not penetrate into the hydrophobic core because it is held back in the headgroup region by electrostatic interactions. Additionally, as we conjectured for PE/PG, H-bonds to PG might also counteract the formation of an interdigitated phase. It is interesting that we found a pronounced thinning of the bilayer in the fluid phase, suggesting that the peptide does indeed insert into the less tightly packed fluid bilayer.

Comparison of the effects on the gel and fluid phases

The effects of LL-37 observed on the gel phase are more straightforward to interpret than those on the fluid phase, but some tendencies are apparent. In the fluid phase, the peptide can be accommodated in the bilayer by filling the void created below the peptide by increased *trans-gauche* isomerization of the hydrocarbon chains of the adjacent lipids. This leads to a thinning of the bilayer, which was first described by Huang's group for magainin in partially hydrated systems (48) and recently also found in fully hydrated liposomal dispersions containing alamethicin (49). In the gel phase, the peptide cannot be accommodated due to the more rigid hydrocarbon chains, and the bilayer rearranges, e.g., by formation of a quasi-interdigitated phase for PG and PC/PG or by disk formation for PC and PC/PS. In the latter cases, the chain melting process is accompanied by a fusion of the lipid disks to larger bilayer sheets, with the peptide residing in the interface (Fig. 5 *B*). The exception to this tendency is PE/PG, where we observe larger fragments in the gel phase and micellar disks in the fluid phase. The fact that the particles are generally smaller above T_m implies that significantly less peptide is situated in the bilayer and more at the disk rims. The driving force for this rearrangement remains to be elucidated.

As a second tendency, pronounced thinning of the fluid-phase membrane (>2 Å) is observed upon peptide interaction with charged bilayers. This seems plausible, considering that in this case the peptide is held more tightly in the headgroup region due to electrostatic attraction and cannot penetrate far into the hydrophobic core. Therefore, the void below the penetrating peptide is larger and the opposing monolayer will have to move closer, leading to a more pronounced thinning compared to neutral PC. Again, PE/PG does not follow this trend as the bilayer thickness is not reduced in the presence of peptide. This, however, is only logical, considering the occurrence of small micellar disks in the fluid phase. If the peptide is situated predominantly at the disk rims, it does not have to be accommodated in the bilayer and therefore does not induce a thinning of the bilayer.

CONCLUSIONS

In model membrane studies, the goal is to create a system that mimics the complex lipid composition of a natural membrane in a simple way, but the question of how simple the model can be made without losing significance must be addressed. In many studies of AMP/membrane interaction, the focal point of consideration is still lipid headgroup charge, which will of course control the affinity of peptides to membranes and will therefore govern specificity. However, although there are some questions left open as to why LL-37 interacts the way it does with the lipid mixtures investigated, we can safely conclude that net charge does not play a dominant role compared to other lipid properties (such as, e.g., H-bonding ability, lipid packing, and hydrocarbon chain length (14)) in determining the mode of lipid/peptide interaction. We definitely do not suggest that LL-37 acts by any of the mechanisms described here in biological systems. We rather show that this peptide displays four different modes of action on the

four phospholipid species predominantly used in model membrane experiments. It also has a different effect on each of the lipid mixtures with identical surface charge (PE/PG, PC/PG, and PC/PS), all of which are used to mimic bacterial cell membranes. The interaction of LL-37 with only binary lipid mixtures is more complicated than expected and does not follow simple rules deduced from its effects on the individual lipids. Thus, our results emphasize how profoundly the choice of the model system can influence the outcome of a study of lipid/peptide interaction and how important it is to try to retain the basic properties (elasticity, charge distribution, dynamics) of the lipid matrix to be mimicked.

SUPPLEMENTARY MATERIAL

To view all of the supplemental files associated with this article, visit www.biophysj.org.

This study was supported by grant P 15657 of the Fonds zur Förderung der wissenschaftlichen Forschung in Österreich and by the Alois Sonnleitner Stiftung, Österreichische Akademie der Wissenschaften.

REFERENCES

1. Lohner, K., editor. 2001. Development of Novel Antimicrobial Agents: Emerging Strategies. Horizon Scientific Press, Wymondham, United Kingdom.
2. Epand, R. M., and R. F. Epand. 2003. Liposomes as models for antimicrobial peptides. *Methods Enzymol.* 372:124–133.
3. Lohner, K., and S. E. Blondelle. 2005. Molecular mechanisms of membrane perturbation by antimicrobial peptides and the use of biophysical studies in the design of novel peptide antibiotics. *Comb. Chem. High Throughput Screen.* 8:241–256.
4. Rothman, J. E., and J. Lenard. 1977. Membrane asymmetry. *Science.* 195:743–753.
5. Wilkinson, S. G. 1988. Gram-negative bacteria. *In* Microbial Lipids. C. Ratledge and S. G. Wilkinson, editors. Academic Press, London. 299–488.
6. O'Leary, W. M., and S. G. Wilkinson. 1988. Gram-positive bacteria. *In* Microbial Lipids. C. Ratledge and S. G. Wilkinson, editors. Academic Press, London. 117–201.
7. Gennis, R. B. 1989. Biomembranes: Molecular Structures and Function. Springer Verlag, New York.
8. de Kruijff, B. 1997. Lipid polymorphism and biomembrane function. *Curr. Opin. Chem. Biol.* 1:564–569.
9. McIntosh, T. J., and S. A. Simon. 1986. Area per molecule and distribution of water in fully hydrated dilauroylphosphatidylethanolamine bilayers. *Biochemistry.* 25:4948–4952.
10. Boggs, J. M. 1987. Lipid intermolecular hydrogen bonding: influence on structural organization and membrane function. *Biochim. Biophys. Acta.* 906:353–404.
11. Matsuzaki, K., K. Sugishita, N. Ishibe, M. Ueha, S. Nakata, K. Miyajima, and R. M. Epand. 1998. Relationship of membrane curvature to the formation of pores by magainin 2. *Biochemistry.* 37:11856–11863.
12. Arnt, L., J. R. Rennie, S. Linser, R. Willumeit, and G. N. Tew. 2006. Membrane activity of biomimetic facially amphiphilic antibiotics. *J. Phys. Chem. B.* 110:3527–3532.
13. Hallock, K. J., D. K. Lee, J. Omnaas, H. I. Mosberg, and A. Ramamoorthy. 2002. Membrane composition determines pardaxin's mechanism of lipid bilayer disruption. *Biophys. J.* 83:1004–1013.
14. Sevcsik, E., G. Pabst, A. Jilek, and K. Lohner. 2007. How lipids influence the mode of action of membrane-active peptides. *Biochim. Biophys. Acta.* 1768:2586–2595.
15. Durr, U. H., U. S. Sudheendra, and A. Ramamoorthy. 2006. LL-37, the only human member of the cathelicidin family of antimicrobial peptides. *Biochim. Biophys. Acta.* 1758:1408–1425.
16. Johansson, J., G. H. Gudmundsson, M. E. Rottenberg, K. D. Berndt, and B. Agerberth. 1998. Conformation-dependent antibacterial activity of the naturally occurring human peptide LL-37. *J. Biol. Chem.* 273:3718–3724.
17. Oren, Z., J. C. Lerman, G. H. Gudmundsson, B. Agerberth, and Y. Shai. 1999. Structure and organization of the human antimicrobial peptide LL-37 in phospholipid membranes: relevance to the molecular basis for its non-cell-selective activity. *Biochem. J.* 341:501–513.
18. Henzler Wildman, K. A., D. K. Lee, and A. Ramamoorthy. 2003. Mechanism of lipid bilayer disruption by the human antimicrobial peptide, LL-37. *Biochemistry.* 42:6545–6558.
19. Pabst, G. 2006. Global properties of biomimetic membranes: perspectives on molecular features. *Biophys. Rev. Lett.* 1:57–84.
20. Amenitsch, H., M. Rappolt, M. Kriechbaum, H. Mio, P. Laggner, and S. Bernstorff. 1998. First performance assessment of the small-angle X-ray scattering beamline at ELETTRA. *J. Synchrotron Radiat.* 5:506–508.
21. Tristram-Nagle, S., R. Zhang, R. M. Suter, C. R. Worthington, W. J. Sun, and J. F. Nagle. 1993. Measurement of chain tilt angle in fully hydrated bilayers of gel phase lecithins. *Biophys. J.* 64:1097–1109.
22. Neville, F., M. Cahuzac, O. Konovalov, Y. Ishitsuka, K. Y. Lee, I. Kuzmenko, G. M. Kale, and D. Gidalevitz. 2006. Lipid headgroup discrimination by antimicrobial peptide LL-37: insight into mechanism of action. *Biophys. J.* 90:1275–1287.
23. Blume, A. 1979. A comparative study of the phase transitions of phospholipid bilayers and monolayers. *Biochim. Biophys. Acta.* 557:32–44.
24. Jing, W., E. J. Prenner, H. J. Vogel, A. J. Waring, R. I. Lehrer, and K. Lohner. 2005. Headgroup structure and fatty acid chain length of the acidic phospholipids modulate the interaction of membrane mimetic vesicles with the antimicrobial peptide protegrin-1. *J. Pept. Sci.* 11: 735–743.
25. Cevc, G., A. Watts, and D. Marsh. 1981. Titration of the phase transition of phosphatidylserine bilayer membranes. Effects of pH, surface electrostatics, ion binding, and head-group hydration. *Biochemistry.* 20:4955–4965.
26. Hauser, H., and G. G. Shipley. 1985. Comparative structural aspects of cation binding to phosphatidylserine bilayers. *Biochim. Biophys. Acta.* 813:343–346.
27. Tardieu, A., V. Luzzati, and F. C. Reman. 1973. Structure and polymorphism of the hydrocarbon chains of lipids: a study of lecithin-water phases. *J. Mol. Biol.* 75:711–733.
28. Pozo-Navas, B., V. A. Raghunathan, J. Katsaras, M. Rappolt, K. Lohner, and G. Pabst. 2003. Discontinuous unbinding of lipid multibilayers. *Phys. Rev. Lett.* 91:028101.
29. Kucerka, N., J. Pencer, J. N. Sachs, J. F. Nagle, and J. Katsaras. 2007. Curvature effect on the structure of phospholipid bilayers. *Langmuir.* 23:1292–1299.
30. Watts, A., K. Harlos, and D. Marsh. 1981. Charge-induced tilt in ordered-phase phosphatidylglycerol bilayers evidence from X-ray diffraction. *Biochim. Biophys. Acta.* 645:91–96.
31. Pabst, G., S. Danner, S. Karmakar, G. Deutsch, and V. A. Raghunathan. 2007. On the propensity of phosphatidylglycerols to form interdigitated phases. *Biophys. J.* 93:513–525.
32. Zhang, Y.-P., R. N. A. Lewis, and R. N. McElhaney. 1997. Calorimetric and spectroscopic studies of the thermotropic phase behavior of the *n*-saturated 1,2-diacylphosphatidylglycerols. *Biophys. J.* 72:779–793.
33. Blume, A. 1993. Dynamic properties. *In* Phospholipid Handbook. G. Cevc, editor. Marcel Dekker, New York. 455–509.
34. Seddon, J. M., and R. H. Templer. 1995. Polymorphism of lipid water systems. *In* Structure and Dynamics of Membranes. R. Lipowsky and E. Sackmann, editors. North-Holland, Amsterdam. 97–160.

35. Thurmond, R. L., S. W. Dodd, and M. F. Brown. 1991. Molecular areas of phospholipids as determined by 2H NMR spectroscopy. Comparison of phosphatidylethanolamines and phosphatidylcholines. *Biophys. J.* 59:108–113.

36. McIntosh, T. J. 1980. Differences in hydrocarbon chain tilt between hydrated phosphatidylethanolamine and phosphatidylcholine bilayers. *Biophys. J.* 29:237–245.

37. Hauser, H., I. Pascher, R. H. Pearson, and S. Sundell. 1981. Preferred conformation and molecular packing of phosphatidylethanolamine and phosphatidylcholine. *Biochim. Biophys. Acta.* 650:21–51.

38. Heller, W. T., K. He, S. J. Ludtke, T. A. Harroun, and H. W. Huang. 1997. Effect of changing the size of lipid headgroup on peptide insertion into membranes. *Biophys. J.* 73:239–244.

39. Lee, M. T., W. C. Hung, F. Y. Chen, and H. W. Huang. 2005. Many-body effect of antimicrobial peptides: on the correlation between lipid's spontaneous curvature and pore formation. *Biophys. J.* 89:4006–4016.

40. Lewis, R. N., and R. N. McElhaney. 2000. Calorimetric and spectroscopic studies of the thermotropic phase behavior of lipid bilayer model membranes composed of a homologous series of linear saturated phosphatidylserines. *Biophys. J.* 79:2043–2055.

41. Petrache, H. I., S. Tristram-Nagle, K. Gawrisch, D. Harries, V. A. Parsegian, and J. F. Nagle. 2004. Structure and fluctuations of charged phosphatidylserine bilayers in the absence of salt. *Biophys. J.* 86:1574–1586.

42. Volles, M. J., and P. T. Lansbury, Jr. 2002. Vesicle permeabilization by protofibrillar α-synuclein is sensitive to Parkinson's disease-linked mutations and occurs by a pore-like mechanism. *Biochemistry.* 41: 4595–4602.

43. Boggs, J. M., H. Y. Wang, G. Rangaraj, and B. Tummler. 1989. Interdigitation of phosphatidylcholine and phosphatidylethanolamine mixed with complexes of acidic lipids and polymyxin B or polymyxin B nonapeptide. *Biochim. Biophys. Acta.* 985:199–210.

44. Mason, J. T., and F. A. Stephenson. 1990. Thermotropic properties of saturated mixed acyl phosphatidylethanolamines. *Biochemistry.* 29: 590–598.

45. Garidel, P., C. Johann, L. Mennicke, and A. Blume. 1997. The mixing behavior of pseudobinary phosphatidylcholine-phosphatidylglycerol mixtures as a function of pH and acyl chain length. *Eur. Biophys. J.* 26:447–459.

46. Garidel, P., and A. Blume. 2000. Miscibility of phosphatidylethanolamine-phosphatidylglycerol mixtures as a function of pH and acyl chain length. *Eur. Biophys. J.* 28:629–638.

47. Murzyn, K., T. Rog, and M. Pasenkiewicz-Gierula. 2005. Phosphatidylethanolamine-phosphatidylglycerol bilayer as a model of the inner bacterial membrane. *Biophys. J.* 88:1091–1103.

48. Ludtke, S., K. He, and H. Huang. 1995. Membrane thinning caused by magainin 2. *Biochemistry.* 34:16764–16769.

49. Pabst, G., S. Danner, R. Podgornik, and J. Katsaras. 2007. Entropy-driven softening of fluid lipid bilayers by alamethicin. *Langmuir.* 23:11705–11711.

50. Israelachvili, J. N., D. J. Mitchell, and B. W. Ninham. 1977. Theory of self-assembly of lipid bilayers and vesicles. *Biochim. Biophys. Acta.* 470:185–201.

51. Sun, W. J., S. Tristram-Nagle, R. M. Suter, and J. F. Nagle. 1996. Structure of gel phase saturated lecithin bilayers: temperature and chain length dependence. *Biophys. J.* 71:885–891.